



Imaging the surface of Mercury using ground-based telescopes

Michael Mendillo^{a, *}, Johan Warell^b, Sanjay S. Limaye^c, Jeffrey Baumgardner^a,
Ann Sprague^d, Jody K. Wilson^a

^aCenter for Space Physics, Boston University, 725 Commonwealth Avenue Boston, MA 02215, USA

^bAstronomiska Observatoriet, Uppsala Universitet, SE-751 20 Uppsala, Sweden

^cSpace Science and Engineering Center, University of Wisconsin, Madison, WI 53706, USA

^dLunar and Planetary Laboratory, University of Arizona, Tucson, AZ 85721, USA

Received 26 October 2000; received in revised form 12 March 2001; accepted 4 May 2001

Abstract

We describe and compare two methods of short-exposure, high-definition ground-based imaging of the planet Mercury. Two teams have recorded images of Mercury on different dates, from different locations, and with different observational and data reduction techniques. Both groups have achieved spatial resolutions of < 250 km, and the same albedo features and contrast levels appear where the two datasets overlap (longitudes 270 – 360°). Dark albedo regions appear as mare and correlate well with smooth terrain radar signatures. Bright albedo features agree optically, but less well with radar data. Such confirmations of state-of-the-art optical techniques introduce a new era of ground-based exploration of Mercury's surface and its atmosphere. They offer opportunities for synergistic, cooperative observations before and during the upcoming Messenger and BepiColombo missions to Mercury. © 2001 Elsevier Science Ltd. All rights reserved.

1. Introduction

In this paper, we compare the first results from two new studies of Mercury's surface that employed the fast digital imaging approach—Baumgardner et al. (2000) and Warell and Limaye (2001), papers hereafter referred to as BMW and W&L, respectively. In contrast to adaptive optics (AO) methods, the approach employed was to use very short exposures in the hope of finding instances when atmospheric turbulence was essentially absent, thus yielding a diffraction limited “perfect seeing” image of the planet. We concentrate on a thorough description of the techniques developed in order to encourage other groups to use relatively simple methods for state-of-the-art studies of Mercury in anticipation of the in situ satellite results to come from Messenger and BepiColumbo, as discussed throughout this special issue.

Imaging the surface of Mercury represents one of the premier challenges in ground-based optical astronomy. The areas of difficulty arise from the planet's proximity to the Sun. Mercury is most often observed during the pre-sunrise or post-sunset times when the planet is near its

maximum separation (elongation) to the west and east of the rising or setting Sun, respectively. Under such conditions, Mercury can be separated from the Sun by up to 28° . Such observations must be made using long, slanted ray paths (large air masses) through the terrestrial troposphere, conditions that generally maximize extinction and scattering of incoming light, as well as poor seeing due to turbulence in the atmosphere. An advantage of this approach is that the background sky is relatively dark, a condition that might allow for AO techniques to be used should a suitable bright guide star be within the field of view. A second possibility is to observe Mercury near mid-day when the air mass is at its minimum. Such attempts have to deal with a bright background sky, the probable lack of a suitable guide star for AO, and solar heating (and hence flexing) of telescope components. All of the above cases have been tried recently, with various degrees of success.

2. Observing strategy considerations

While the BMW and W&L papers used very different data analysis techniques, their observations were based on the same short-exposure, turbulence-minimizing philosophy described in detail by Fried (1978). Briefly, turbulence may be treated as atmospheric blobs of characteristic dimension r .

* Corresponding author. Tel.: +1-617-353-5990; fax: +1-617-353-6463.

E-mail address: mendillo@bu.edu (M. Mendillo).

These atmospheric density irregularities distort wave fronts resulting in an image with spatial resolution degraded from its theoretical diffraction limit (λ/D) for a telescope with aperture D . Fried (1978) discusses a “turbulence-limited” resolution which arises from the blob dimension along the ray path (r_0) to be λ/r_0 , a figure of merit that can increase to $\lambda/(3.4r_0)$ for very short exposures. Fried then relates r_0 and D by computing the probability of getting a “good short exposure” image:

$$\text{Prob} \sim 5.6 \exp[-0.1557(D/r_0)^2]. \quad (1)$$

Eq. (1) points to the interesting result that for a fixed scale of turbulence (r_0), the probability of a good image decreases dramatically as the aperture (D) of the telescope increases. For example, with $D/r_0 \sim 5$, ten “short exposure” images would yield one “good” image, while at $D/r_0 \sim 10$, a million “short exposures” are needed for one “good” image.

To define quantitatively a “good image”, Fried adopts a change in wave front tilt of less than $\frac{1}{2}(\lambda/D)$. He then goes on to relate the exposure time (t) for this criterion for a good image to the turbulence scale length (r_0) and the wind speed (V) perpendicular to the ray path as

$$t = \frac{1}{2}r_0/V. \quad (2)$$

There are some interesting implications of Eq. (2). Clearly, it is the onset of small-scale turbulence ($r_0 \rightarrow 0$) that precludes long exposures. This is the condition that favors pre-dawn observations, before turbulence develops. For a target near zenith, V is the local horizontal wind; thus small daytime winds would be the requirement for relatively long exposure times for Mercury. For a target at large zenith angles, such as Mercury at prior to sunrise, V would be upwelling/downwelling motions near the telescope. This is the second condition that favors pre-dawn observations, before grazing sunlight sets the local atmosphere into vertical motion.

The BMW data were taken near sunrise, conditions designed to exploit the capabilities of a large telescope ($D = 1.5$ m) for light gathering power and high resolution, hoping to avoid small-scale turbulence (r_0) and vertical winds (V) that would limit the probability of obtaining a good image from such a large aperture instrument. A fixed short-exposure time of 17 ms was used for these measurements on 29 August 1998 at the 1.5 m Mt. Wilson telescope in California.

The W&L results came from a telescope with $\frac{1}{3}$ rd the aperture ($D = 0.5$ m), the Swedish Vacuum Solar Telescope (SVST) on La Palma in the Canary Islands. Eq. (1) shows that the SVST could thus cope with more smaller scale turbulence than the Mt. Wilson instrument. This allowed images to be obtained with Mercury over a far greater range of elevation angles (18–80°). Exposure times of 25–360 ms were used at La Palma.

3. Observations and image processing

The data acquisition methods employed by the two groups differed in several ways. W&L made their initial selection of images in real time using a rapid assessment of contrast algorithm. Thus, from five observing runs totaling 28 days from 1995 to 1999, approximately 250,000 exposures were made and 5000 were auto-selected and saved to disk. These CCD images were either in an 8-bit 1035×1360 pixel format or a 10-bit 1032×1536 format. Subsequently, 140 images were processed and used in their analysis.

The BMW group stored to disk all 219,000 exposures made during a single ~ 60 min run on 29 August 1998. Only a 130×130 pixel region of interest (ROI) that contained Mercury (using real-time ROI manual tracking) was saved from each of the 512×512 pixel, 8-bit exposures. They subsequently used an automatic contrast assessment scheme to rank all 219,000 images, eventually using two sets of 30 images with the highest contrast scores to portray final results.

With “best images” selected, both groups again used rather different schemes of image processing of their selected frames. The W&L method was a rigorous use of bias, dark, flat field and calibration frames. They cropped their array to 512×512 pixels centered on the calculated center of the planet. Hot pixels were removed, sky background subtracted, and the image intensity was normalized for a zero level mean sky brightness, and unity for the brightest point on the disk. To reduce noise and enhance detail, the selected frames were Wiener filtered and then subjected to unsharp masking, a procedure that effectively enhanced small-scale detail and increased the contrast between dark and bright regions. The 140 processed images were then used as independent data sets to generate a global map of Mercury.

The BMW group used a less standard reduction scheme, due mainly to the fact that the pilot study nature of the observations was more concerned with testing the rapid data storage algorithm at the expense of bias, dark, flat field and star images. All 219,000 raw data images were first smoothed to reduce pixel-to-pixel noise. An operator was then applied to characterize the contrast in the vicinity of each pixel, and then the resulting contrast values were squared to enhance small regions of high contrast (e.g., the limb) over large regions of low contrast (i.e., shades of gray across portions of the surface illuminated by sunlight). Finally, the contrast scores of all the pixels in the 130×130 ROI arrays were summed to get a single sharpness score for that image.

The top 1000 scored images were then tested for “rubber sheeting” distortions by comparing each image with the known geometric shape of Mercury on 29 August 1998. The top 30 images obtained in this way (with Mercury in one orientation on the detector) were then sub-pixel shifted by keying on the highest score image; with all 30 images so registered, they were co-added. Next, the process was repeated

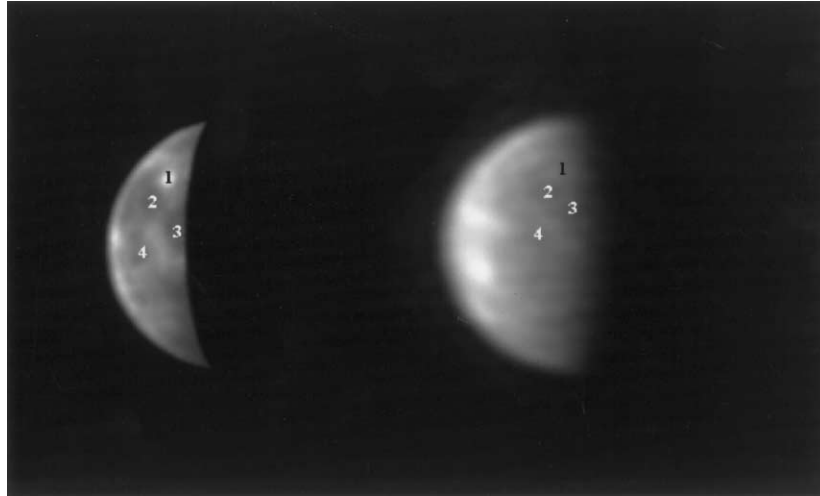


Fig. 1. Comparison of the two observational methods. (left) BMW image taken on August 29, 1998, showing longitudes $\sim 270\text{--}330^\circ$. The effects of varying solar illumination have been removed from this image and the contrast has been increased to enhance features. (right) W&L image taken on October 22, 1995, showing longitudes $\sim 270\text{--}360^\circ$. Four features have been numbered in both images for visual comparison.

with the top 30 images of Mercury at a different orientation on the chip. These effectively $\frac{1}{2}$ s time exposures, obtained by the shift-and-add of only the “best” frames, were sharpened using a maximum entropy method of deconvolving a point-spread function (PSF) from the image. Since no star was observed simultaneously within the ROI containing Mercury, the limb profile of the co-added images was used to estimate the initial PSF. The choice of a Gaussian profile with a HPFW of 4 pixels was used that effectively determined the spatial resolution achieved to be ~ 250 km. The two independent images were then aligned and added. Finally, the resulting image was divided by the square root of the cosine of the local solar zenith angle to correct for different lighting conditions over the surface. The effect of this was to reduce limb brightening, a prominent aspect of the raw data images.

4. Results

Fig. 1 shows the best images obtained by the BMW (left) and W&L (right) groups for the same portion of Mercury. The longitudes sampled were $270\text{--}330$ (left) and $270\text{--}360$ (right), regions of the planet not imaged during the Mariner 10 fly-bys in 1974–75. The similarities between these two independent images are remarkable in many ways. As described earlier, the data taking and analysis protocols were entirely different, and yet comparable results were obtained. The telescope apertures differed by a factor of three, and yet the resolutions obtained are comparable ($\sim 200\text{--}250$ km). Several features away from the limb are numbered to aid in comparison of albedo features on the disk. In the northern hemisphere, a bright feature (#1) and a few dark areas (#2–4) are seen clearly in both images. In the southern hemisphere, the albedo signatures are

less well apparent in both data sets. The albedo variations seen in the two data sets appear to be consistent for regions away from the limb. Recall that both groups treated limb brightening in different ways. The surface contrast in the solar-illumination-corrected BMW image is 10–15% over most of the imaged region, with one feature 30% brighter than its surroundings. The W&L images, which have not been corrected for illumination, have surface contrasts of 25–35% over the whole surface, while the contrast obtained along 1° meridian swaths (where solar illumination effects are reduced) is $14 \pm 8\%$, in close agreement with the BMW values.

We note that the observations made by the BMW group were done jointly with Dantowitz et al. (2000). The output of a single camera was sent simultaneously to a digital recording system (Baumgardner et al., 2000) and to an analog videotape recorder (Dantowitz et al., 2000). The analog data were played back for visual selection of the “good” frames by the lead author, and 40 frames from a 10-min portion of the total dataset were averaged. Their results (Fig. 2 in Dantowitz et al., 2000) displayed with the same journal printing methods as the BMW image appear less satisfactory than shown here in Fig. 1. Of particular concern is the lack of detail in the southern hemisphere, and the dominance of limb brightness in both hemispheres. Thus, while a valiant effort was made using subjective data reduction of analog data, the end result falls short of using digital data and more advanced imaging processing methods.

5. Discussion

In order to compare the quantitative locations of albedo features shown in Fig. 1, we use Fig. 2 to portray Mercury’s surface in a cylindrical projection. The top panel

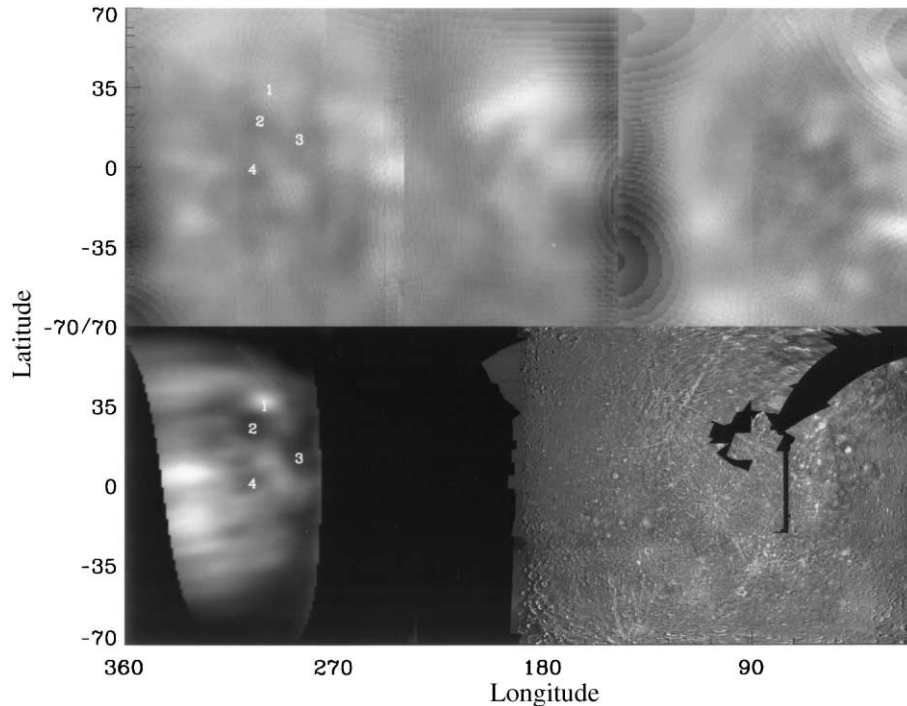


Fig. 2. Global cylindrical projection maps of Mercury. (top) Complete map from ground-based images of W&L. (bottom right) Mariner 10 data (courtesy of A. Tayfun Oner) combined with BMW image (bottom left). The same albedo features labeled in Fig. 1 are indicated.

gives the full set of longitudes obtained from the multi-year study at SVST on La Palma (Warell and Limaye, 2001). Using such a format, the W&L study investigated the details of the site-by-site comparisons of albedo features with Mariner data. Their global results represent a milestone in ground-based observations of planet Mercury. The lower panel shows the single image obtained at Mt. Wilson by Baumgardner et al. (2000), together with the high resolution results obtained by Mariner 10 (courtesy of A. Tayfun Oner) to show the hemisphere viewed from space.

We concentrate here on the comparison of the first set of optical wavelength images of Mercury for longitudes between 270° and 360° . Overall, the images give the appearances of regions of low albedo maria and higher albedo highlands with some freshly impacted excavation regions similar to the appearance of the Earth-facing disk of the Moon at similar spatial resolution. It is tempting to conclude that such an interpretation is correct. However, historically, much debate and no conclusive evidence has been available from Mariner 10 imaging (cf. Spudis and Guest, 1988 and references therein) and ground-based radar imaging (cf. Clark et al., 1988; Harmon and Campbell, 1988) for volcanics on Mercury. A recent reanalysis of the three-color Mariner 10 images of Mercury by Robinson and Lucey (1997) has greatly increased our understanding of the diversity of materials present on the surface, with good evidence for pyroclastic deposits and lava flows. Viewed in that context, and by inference with the Moon, features 2–4 may indeed be compositionally distinct from the surrounding terrain and be

a result of some differentiated magmatic event or events. More imaging of the type achieved here, using multi-wavelength filters designed for compositional remote sensing, may be able to answer this question at all longitudes on the planet.

The longitudes in the images presented here have also been imaged at 3.5 cm (X band) with the Goldstone 70-m antenna transmitting and 26 antennas of the very large array (VLS) receiving (Harmon and Slade, 1992; Slade et al., 1992; Butler et al., 1993). Figs. 6 and 11 of Butler et al. (1993) display detailed images and mercator projections of radar residuals in both same sense (SS) and opposite sense (OS), following removal of a standard radar reflectivity model. This treatment permits high contrast for displaying variations in SS and OS radar reflectivity. Feature 1 (centered at $\sim 38^\circ, 298^\circ$), the highest albedo and most discrete feature in the image of BMW, is barely visible in that of W&L, probably because of differences in illumination. Although the region around this location of feature 1 displays highly variable SS reflectivities, generally it corresponds to medium strength SS and OS reflectivities. No distinctive signal is apparent. Dark albedo features 2–4 (centered at $\sim 15^\circ, 285^\circ; 0^\circ, 305^\circ; \text{ and } 26^\circ, 305^\circ$, respectively) are located in regions of low SS and OS residuals. Regions which are highly cracked and fractured will have enhanced SS and OS backscatter because of multiple scattering at the surface and subsurface (Butler et al., 1993). Thus, the dark albedo regions 2–4 correspond to relatively smooth terrain.

Along Mercury's limb in Fig. 1 (in which Mercury in the right panel has rotated $\sim 20^\circ$ of longitude east relative to that in the left) are some relatively bright regions. An equatorial spot ($\sim 3^\circ, 331^\circ$) corresponds well with a localized SS enhancement noted by Butler et al. (1993). In addition, radar bright spot A ($\sim -27^\circ, 348^\circ$) shows up as a bright albedo feature in the image of W&L. Because of illumination geometry, it is not clear if radar bright spot B ($55^\circ, 345^\circ$) causes the fuzzy bright region in that vicinity. Radar spots A and B correspond to locations where enhancements have been observed in Mercury's Na atmosphere (for a detailed discussion see Sprague et al., 1998).

6. Summary

We have compared two independent attempts to image Mercury's surface and find a remarkable degree of agreement. For longitudes not sampled by Mariner 10, these represent the first detections and confirmations of significant albedo features at optical wavelengths on that side of the planet. We find that some features can be matched with features observed in 3.5 cm radar imaging. Three low albedo regions correspond to relatively low radar reflectivity and thus smooth terrain. By using such techniques along with narrow bandpass filters especially chosen for geochemical discrimination, we hope to determine compositional differences on the surface, and thus enhance our understanding of the evolution of Mercury's surface. In addition, it will also be possible to study the distribution of sodium, potassium, and calcium in the atmosphere above Mercury's surface.

Acknowledgements

The Baumgardner et al. (2000) observations were made at the Mount Wilson Observatory in California during a joint observing run with staff from the Boston Museum of Science. Funding for instrumentation development in high definition imaging was provided by the Office of Naval Research. The observational and analysis efforts

were supported by seed research funds provided by Boston University to the Center for Space Physics. The Warell and Limaye (2000) research program has been funded partly by the Swedish Natural Science Research Council and by the Anna and Allan Lofberg Foundation. The Swedish Vacuum telescope is operated on the island of La Palma by the Royal Swedish Academy of Sciences in the Spanish Observatorio del Roque de los Muchachos of the Instituto de Astrofísica de Canarias.

References

- Baumgardner, J., Mendillo, M., Wilson, J.K., 2000. A digital high definition imaging system for spectral studies of extended planetary atmospheres: 1. Initial results in white light showing features on the hemisphere of Mercury unimaged by Mariner 10. *Astron. J.* 119, 2458–2464.
- Butler, B., Muhleman, D., Slade, M.A., 1993. Mercury: full-disk radar images and the detection and stability of ice at the north pole. *J. Geophys. Res.* 98, 15,003–15,023.
- Clark, P.E., Leake, M.A., Jurgens, R.F., 1988. Goldstone radar observations of Mercury. In: Vilas, F., Chapman, C., Matthews, M. (Eds.), *Mercury*. University of Arizona Press, Tucson, AZ.
- Dantowitz, R.F., Teare, S.W., Kozubal, M.J., 2000. Ground-based high-resolution imaging of Mercury. *Astron. J.* 119, 2455–2457.
- Fried, D.L., 1978. Probability of getting a lucky short-exposure image through turbulence. *J. Opt. Soc. Am.* 68, 1651–1658.
- Harmon, J.K., Campbell, D.B., 1988. Radar Observations of Mercury. In: Vilas, F., Chapman, C., Matthews, M. (Eds.), *Mercury*. University of Arizona Press, Tucson, AZ.
- Harmon, J.K., Slade, M.A., 1992. Radar mapping of Mercury: full-disk images and polar anomalies. *Science* 258, 640–642.
- Robinson, M.S., Lucey, P.G., 1997. Recalibrated Mariner 10 color mosaics: implications for mercurian volcanism. *Science* 275, 197–200.
- Slade, M., Butler, B., Muhleman, D.O., 1992. Mercury radar imaging: evidence for polar ice. *Science* 258, 635–640.
- Sprague, A.L., Schmitt, W.J., Hill, R.E., 1998. Mercury: sodium atmospheric enhancements, radar bright spots, and visible surface features. *Icarus* 135, 60–68.
- Spudis, P., Guest, J., 1988. Stratigraphy and geologic history of Mercury. In: Vilas, F., Chapman, C., Matthews, M. (Eds.), *Mercury*. University of Arizona Press, Tucson, AZ, pp. 118–164.
- Warell, J., Limaye, S.S., 2001. Properties of the Hermean Regolith: 1. Global Regolith Albedo variation at 200 km scale from multicolor CCD imaging. *Planet. Space Sci.*, 20, this issue.